Electronic Supplementary Material (ESI) for New Journal of Chemistry.

MOF-derived CoP/CuP hybrids as a bifunctional electrocatalyst for zinc–air batteries

Huimin Liu[a], Xing Zong[b], Yongfei Wang[a,b]*, Zhizhi Hu[a], Zhiqiang Zhang[a]*

[a]School of Chemical Engineering, University of Science and Technology Liaoning 185 Qianshan Zhong Road, Anshan 114051, P. R. China
[b]School of Materials and Metallurgy, University of Science and Technology Liaoning Anshan, Liaoning 114051, P. R. China
E-mail: wyf8307@ustl.edu.cn, zzq@ustl.edu.cn

Experimental Section

Materials

Copper nitrate hexahydrate ($Cu(NO_3)_2·3H_2O$, AR) and methanol (CH_3OH, AR) were purchased from Sinopharm Chemical Reagent Co., Ltd. 2-Methylimidazole ($C_4H_6N_2$, 98%) and Sodium hypophosphite (NaH_2PO_2, AR) were purchased from Aladdin® Co., Ltd. Cobalt nitrate hexahydrate ($Co(NO_3)_2·6H_2O$, AR) was bought from Macklin Biochemical Co., Ltd.

Synthesis of CuCo-ZIF and derived Co/Cu@NC.

2-methylimidazole (1.23 g), $Co(NO_3)_2·6H_2O$ (0.73 g) and $Cu(NO_3)_2·3H_2O$ (0.15 g) were dissolved separately in 25, 10, 10 mL of methanol solution, then slowly mixed them and ultrasonic treatment for 20 min to make them fully react, after which time the resulting precipitate was left for 24 h. Next, the solution was centrifuged (10000 rpm×10 min), washed with methanol, and vacuum dried at 60 ℃ to obtained CuCo-ZIF. Finally, as-obtained CuCo-ZIF was placed in a porcelain boat and heated to 900 ℃ under N_2 flow for 2 h to

yield Co/Cu@NC. Co@NC was synthesized under similar conditions to visualize the role of the Cu species.

Synthesis of CoP/CuP@NC

The above obtained Co/Cu@NC (0.3 g) were put into the tube furnace and the phosphorous precursor of NaH_2PO_2 (0.1 g) was placed in front of the Co/Cu@NC, which was then directly used for pyrolysis to obtain CoP/CuP@NC. The synthetic procedure of CoP@NC was similar to that of CoP/CuP@NC, except for using Co@NC as the precursor.

Characterization

The external micro morphology of the powder catalyst material was analyzed by field-emission scanning electron microscopy (FESEM, ZEISS SIGMA 500), and the shape and size dispersion of the material were observed. The transmission electron microscopy (TEM) and high-resolution TEM (HR-TEM) images were obtained on a thermal-field emission microscope (JEM ARM200F). The composition and corresponding element distribution of the materials were detected by the high-angle annular dark-field scanning TEM (HAADF-STEM, JEOL JEM-2100F) and corresponding energy dispersive X-ray (EDX) spectra. X-Ray powder diffraction (XRD, Bruker D8 Discovery XRD) with Cu Ka radiation (λ = 1.5406 Å) was used to analyze the crystal structure of the catalyst. The Raman spectra was obtained on a Bruker spectrometer equipped with a 532 nm laser excitation.The chemical element environment on the surface of the catalyst sample was analyzed by X-ray photoelectron

spectroscopy (XPS, Kratos AXIS Supra) equipped with Al K alpha. Qualitative or semi quantitative analysis is performed on the catalyst sample to obtain the valence and valence information of the elements in the catalyst material. The pore structural information of the materials was explored via the N_2 adsorption-desorption measurement (Quantachrome Instruments Version 4.00). All the samples were degassed in a vacuum at 473 K and then measured at 77 K. The specific surface area was obtained based on the Brunauer-Emmett-Teller (BET) model.

Electrochemical measurements

The electrocatalytic performance of all samples was measured using an electrochemical workstation (Ivium Vertex. One. EIS). ORR and OER electrocatalytic reactions were measured in a standard three electrode system at room temperature. Apply the prepared catalyst ink (catalyst loading of 0.21 mg cm^{-2}) evenly on a glassy carbon working electrode (RDE) with an area of 0.196 cm^{-2}, with Ag/AgCl (3.5 M KCl) electrode as the reference electrode and platinum mesh as the counter electrode. For catalysts inks used in the electrochemical measurements were prepared by dispersing 5 mg of catalyst powder in the mixture solution (490 μL ethanol, 490 μL deionized water and 20 μL Nafion (5 wt%)) and then sonicating for 30 min to form homogeneous catalyst inks. All potentials were converted into reversible hydrogen electrode (RHE) potentials by conversion formula ($E_{RHE}=E_{Ag/AgCl}$ + 0.0591 × pH + 0.198). ORR tests were performed in 0.1 M KOH soluton. RDE measurement was

first conducted by linear sweep voltammetry (LSV) in N_2 saturated aqueous solution to measure the background current. Then the electrolyte medium was purged with high purity O_2 to guarantee O_2-saturated electrolytic environment. LSV curves were conducted with the potential range from 0.1 to -1 V at different rotating speeds (100, 400, 900 and 1600 rpm) with a scan rate of 5 mV s^{-1}. OER tests were performed in 1 M KOH soluton. LSV curves were conducted with the potential range from 0 to 1.2 V at 1600 rpm with a scan rate of 5 mV s^{-1}. The function of C_{dl} is to evaluate the electrochemical active surface area (ECSA) of catalysts, which can be obtained by cyclic voltammetry (CVs) at different scan rates (10−100 mV s^{-1}) in a non-Faradaic region (0−0.15 V). Electrochemical impedance spectroscopy (EIS) measurements were conducted in the frequency range of 100 KHz to 0.01 Hz, with an amplitude of 5 mV and a potential of 1.6 V vs. RHE. Stability tests was carried out by chronopotentiometry with continuously supplying oxygen (in 0.1 M KOH at a constant current density of -0.1 mA cm^{-2} for ORR and in 1 M KOH at a constant current density of -10 mA cm^{-2} for OER)

Zn–Air Battery Assembly and Measurements

The polished zinc plate was used as the anode of the Zn–air battery, the catalyst coated on carbon paper as the cathode and the electrolyte was 6 M KOH solution containing 0.2 M $ZnCl_2$. The total load of cathode catalyst was 0.5 mg cm^{-2}. The performance of zinc–air battery was evaluated using the CT3001A battery testing system (Wuhan Landian Electronics Co. Ltd., China).

The galvanostatic discharge/charge cycling stability was performed at an alternating current density of 5 mA cm^{-2} with a cycling interval of 10 min (5 min for discharging and 5 min for charging).

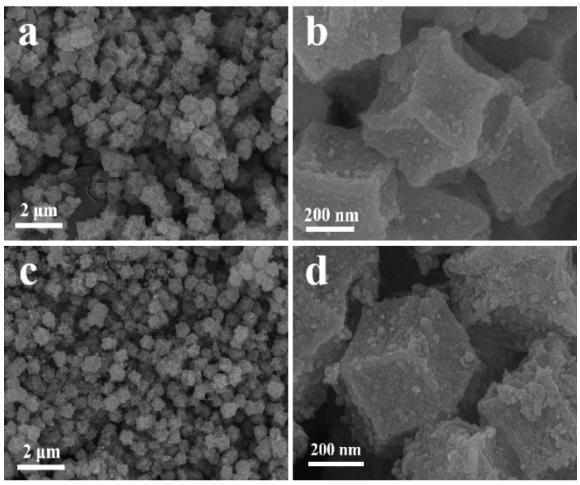

Fig. S1. SEM images at different magnifications of (a,b) Co/Cu@NC and (c,d) CoP/CuP@NC.

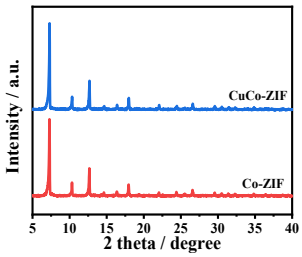

Fig. S2. XRD pattern of CuCo-ZIF and Co-ZIF.

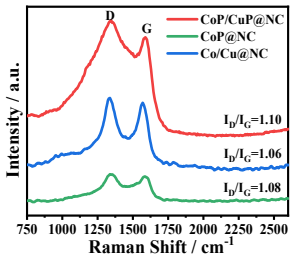

Fig. S3. Raman spectra of CoP/CuP@NC, CoP@NC, and Co/Cu@NC.

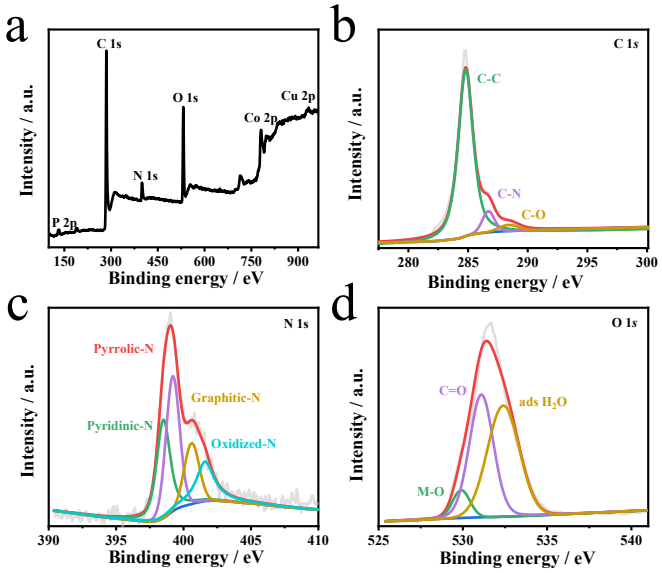

Fig. S4. (a) XPS spectra, (b) C1s, (c) N1s and (d) O 1s of the CoP/CuP@NC.

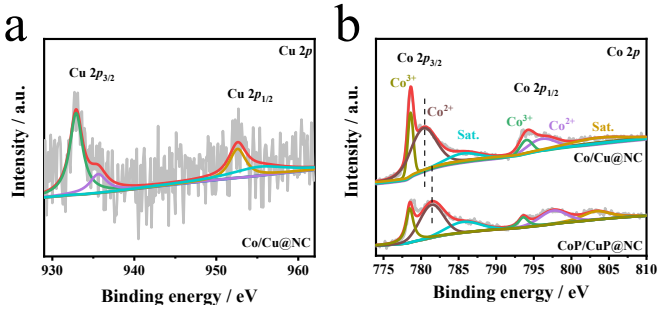

Fig. S5. (a) High-resolution XPS spectra of Cu 2p of Co/Cu@NC. (b) High-resolution XPS spectra of Co 2p of Co/Cu@NC and CoP/CuP@NC.

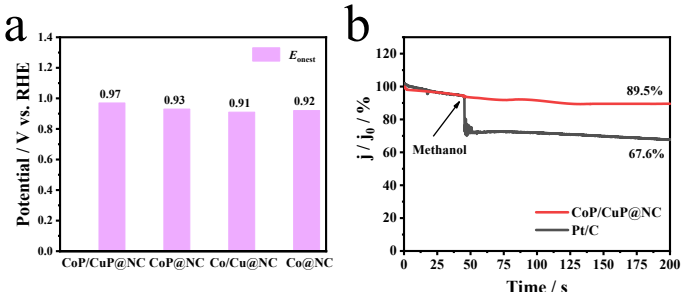

Fig. S6. (a) Comparison of E_{onset} of CoP/CuP@NC and the compared samples in 0.1 M KOH electrolyte. (b) Methanol resistance test of CoP/CuP@NC and Pt/C.

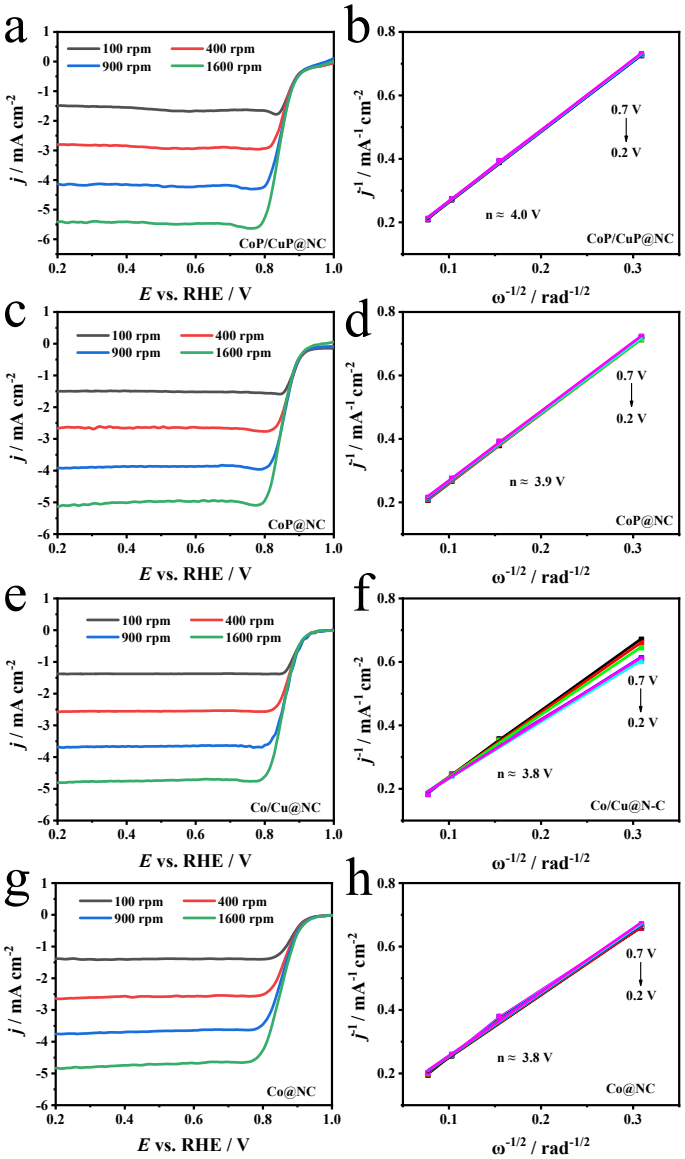

Fig. S7. LSV curves at different rotation rates and corresponding Koutechy−Levich (K−L) plots of (a,b) CoP/CuP@NC, (c,d) CoP@NC, (e,f) Co/Cu@NC, (g,h) Co@NC.

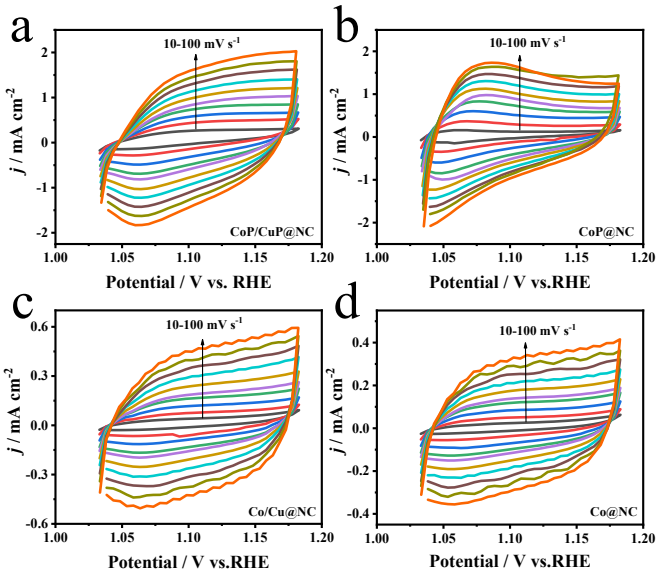

Fig. S8. CV curves of (a) CoP/CuP@NC, (b) Co@NC, (c) Co/Cu@NC and (d) Co@NC at different scan rates.

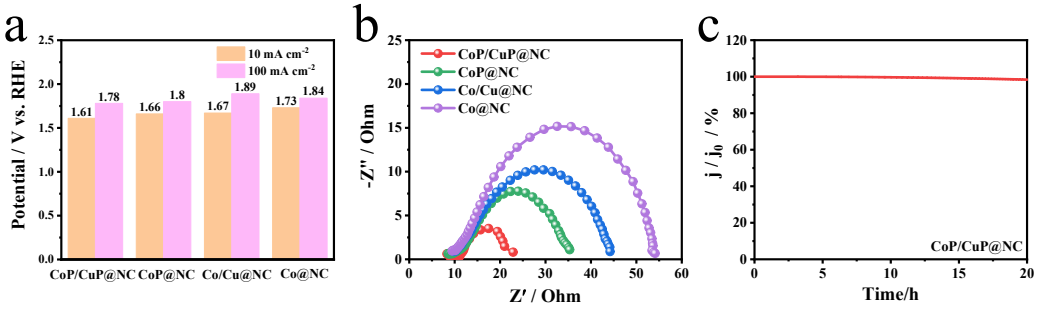

Fig. S9. (a) Comparison of E_{j10} and E_{j100} of CoP/CuP@NC and the compared samples in 1 M KOH electrolyte. (b) The Nyquist plots of CoP/CuP@NC and control samples. (c) OER stability of CoP/CuP@NC.

Table S1. Comparison the ORR activity of CoP/CuP@NC with mentioned in this paper

catalysts in 0.1 M KOH solutions.

Catalyst	E_{onset} (V)	$E_{1/2}$ (V)	J_L (mA cm^{-2})	Tafel slope (mV dec^{-1})
Pt/C	0.91	0.87	-5.2	30
CoP/CuP@NC	0.97	0.86	-5.4	38
CoP@NC	0.93	0.84	-5.1	39
Co/Cu@NC	0.91	0.83	-4.9	84
Co@NC	0.92	0.83	-4.8	84

Table S2. Comparison the OER activity of CoP/CuP@NC with mentioned in this paper catalysts in 1 M KOH solutions.

Catalyst	E_{10} (mV)	E_{100} (mV)	Tafel slope (mV dec^{-1})
RuO_2	1.53	1.71	98
CoP/CuP@N-C	1.61	1.78	68
CoP@N-C	1.65	1.80	69
Co/Cu@N-C	1.65	1.89	92
Co@N-C	1.67	1.84	113

Table S3. Comparison the bifuntional activity of CoP/CuP@NC with other transition metal-based catalysts.

Catalyst	$E_{1/2}$ (mV)	E_{10} (mV)	ΔE (mV)	Ref
CoP/CuP@NC	**0.86**	**1.61**	**0.75**	**This work**
NixP-NP-C	0.76	~1.75	~0.99	Appl. Cataly. B-Environ. 2023, 321, 122041.
FeNiP/NPCS	0.84	1.548	0.708	Chem.Eng. J. 2020, 389 124408.
H-CNP@M	0.833	1.524	0.691	Chinese Chem. Lett. 2023, 108318

Co@NC	0.824	1.613	0.789	J. Mater. Chem. A 2023, 11, 15006.
Fe SAs LS	0.79	1.63	0.84	Angew. Chem. Int. Ed. 2023, 62, e202304229
Co-N-$P_{1.5}$-MC	0.84	1.645	0.805	Nano Res. 2023, 16, 5887.
Cu-Co_2P/CNFs	0.792	1.59	1.798	Nanotechnology 2022, 33, 135202.
CoO/CoP FNS	0.81	1.595	0.785	Small *2019, 15,* 1904210.
CoC_x/$(Co_{0.55}Fe_{1.945})_2$P@C	0.84	1.62	0.78	J. Colloid Interf. Sci. 2021, 590, 321.